CCFE
CULHAM CENTRE FOR FUSION ENERGY

UK Atomic Energy Authority

UKAEA-CCFE-CP(23)49

R. B. Morales, A. Salmi, P. Abreu, C. H. S. Amador, P. Carman, J. Fessey, J. Flanagan, M. Fontana, C. Giroud, S. Hacquin, S. Heuraux, L. Meneses, R. Sabot, A. Silva, A. Sirinelli, G. Szepesi, D. Taylor, D. Terranova.

Improved accuracy and robustness of electron density profiles from JET's FMCW reflectometers

Improved accuracy and robustness of electron density profiles from JET's FMCW reflectometers

R. B. Morales, A. Salmi, P. Abreu, C. H. S. Amador, P. Carman, J. Fessey, J. Flanagan, M. Fontana, C. Giroud, S. Hacquin, S. Heuraux, L. Meneses, R. Sabot, A. Silva, A. Sirinelli, G. Szepesi, D. Taylor, D. Terranova.

This paper has been submitted to
15th International Reflectometry Workshop for fusion plasma diagnostics,ITER Council Room, 7 - 10 June 2022

Improved accuracy and robustness of electron density profiles from JET's FMCW reflectometers

R.B.Morales[1], A.Salmi[2], P.Abreu[3], C.H.S.Amador[4], P.Carman[1], J.Fessey[1], J.Flanagan[1], M.Fontana[1], C.Giroud[1], S.Hacquin[5], S.Heuraux[6], L.Meneses[7], R.Sabot[5], A.Silva[3], A.Sirinelli[7], G.Szepesi[1], D.Taylor[1] and D.Terranova[8]

EUROfusion Consortium, JET, Culham Science Centre, Abingdon, OX14 3DB, UK

[1]*UKAEA, Culham Centre for Fusion Energy, Culham Science Centre, Abingdon, Oxon, OX14 3DB, UK*

[2]*VTT, P.O. Box 1000, FI-02044 VTT, Espoo, Finland*

[3]*IPFN, Instituto Superior Técnico da Universidade de Lisboa, 1049-001 Lisboa, Portugal*

[4]*UTFPR, Department of Natural Sciences, Cornélio Procópio - Brazil*

[5]*IRFM, CEA Cadarache, 13108 Saint-Paul-lez-Durance, France*

[6]*IJL, University of Lorraine, UMR 7198 CNRS, BP 50840, 54011 Nancy Cedex, France*

[7]*ITER Organization, Route de Vinon, CS 90 046, 13067 Saint Paul Lez Durance, France*

[8]*Consorzio RFX and ISTP-CNR, Corso Stati Uniti 4 - 35127 Padova, Italy*

1 Introduction

JET's frequency-modulated continuous-wave (FMCW) reflectometers have been operating well with the current design since 2005 and density profiles are being automatically calculated intershot since then[1]. However, the calculated profiles had long suffered from several shortcomings – poor agreement to other diagnostics; sometimes inappropriately moving radially by several centimetres; elevated level of radial jitter; and persistent wriggles (strong unphysical oscillations in the reconstructed density profiles), sometimes associated, but not exclusive, to band junctions. This contribution goes through several aspects modified in the data analysis that resulted in significant suppression of all these issues.

All optimized variables that impact the quality of the reconstructed density profiles are connected to the recursive profile reconstruction formula that can be written as

$$R_n = R_{n-1} + \frac{1}{W}\frac{\Delta\varphi_{pla}(f_n)}{N_{R_{n-1}}(f_n, f_{pe}, f_{ce})}, \tag{1}$$

with R_n being the next cut-off position to be calculated, R_{n-1} the previous already calculated cut-off position, W the weight factor which is typically a constant 2/3[2, 3], but can be optimized to match the shape of the refractive index [4], $N_{R_{n-1}}(f_n, f_{pe}, f_{ce})$ the refractive index for frequency f_n at position R_{n-1} and $\Delta\varphi_{pla}$ being the phase increment from propagation along the plasma due to a probing frequency step f_{n-1} to f_n, which is computed as

$$\Delta\varphi_{pla}(f_n) = \Delta\varphi_{meas}(f_n) - \Delta\varphi_{ref}(f_n) + \Delta\varphi_{vac}(f_n), \tag{2}$$

where $\Delta\varphi_{meas}(f_n)$ is the total phase increment measured, $\Delta\varphi_{ref}(f_n)$ the reference vacuum phase increment measured before plasma and $\Delta\varphi_{vac}(f_n)$ the excess vacuum propagation phase increment subtracted with the reference that needs to be added back numerically as calculated by

$$\Delta\varphi_{vac}(f_n) = \frac{4\pi(f_n - f_{n-1})}{c}(R_{wall} - R_0), \tag{3}$$

with R_0 being the initial profile reconstruction position (initialization position), R_{wall} the position at which the probing beam is reflected at the inner-wall during the reference measurement and c the speed of light in vacuum.

First and foremost, X-mode profiles can only be as radially accurate as the magnetic field profile provided from the equilibrium reconstruction. This is because the reconstructed cut-off profile is anchored to the f_{ce} profile at the initialization step (determination of R_0). Eq. 3 shows how the R_0 is used in the calculation of the phase increment for every probing frequency step, and therefore every reconstructed cut-off position from Eq. 1. The advances in the equilibrium reconstruction that provide the f_{ce} profile input are reported in Sec. 2.

Eq. 3 also shows a contribution from R_{wall}, the inner-wall reflection position. Due to the intricate topology in that region, ray-tracing calculations were performed to reveal the location where the detected waves come from. The resulting positions and impact on reconstructed profiles are reported in Sec. 3.

Because the injected waves start being reflected at very low densities, resulting in initialization of the profile reconstruction (determination of R_0 in Eq. 3) very close to the vessel outer-wall, the ripple effect in the magnetic field profile has been estimated and implemented in the profile reconstruction algorithm, leading to further improving the agreement of the radial location of reconstructed profiles to other diagnostics, as discussed in Sec. 4.

A position benchmarking revealed higher discrepancies with the low field measurements which are associated with the use of the Q-band in the plasma edge. Further optimizations that suppressed this behaviour were the accuracy of saved sweep-time parameter (optimization between the values requested and actually used by the oscillator) and optimized filtering and fitting of the vacuum reference signal ($\Delta\varphi_{ref}(f_n)$ in Eq. 2). These optimizations are discussed in Sec. 5.

All improvements discussed above address the absolute radial position of the reconstructed profiles, but they also suffer from strong radial jitter due to spurious reflections and strong radial oscillations. The former has been improved with the implementation of the burst mode analysis[5] and the latter with oscillation reducing calibrations, as discussed in Sec. 6, also including another radial position benchmark after all aforementioned improvements, followed by conclusions and prospects in Sec. 7.

2 Progress in equilibrium reconstruction

Since the beginning of the reflectometers operation, a large discrepancy has been observed on the expected radial location of the reconstructed density profiles. Because the magnetic field profile from the equilibrium reconstruction also suffered from strong imprecisions (initially mostly at the toroidal field component), the location of reflectometer profiles was being adjusted with a correction factor on the input toroidal magnetic field. This correction was routinely performed as a validation step for the reflectometry profiles. The installation of a LKCO system (High Accuracy Bi-directional DC AC Fiber Optic Current Measurement) has enabled much more accurate toroidal field measurements, but it was only when the FLUSH equilibrium access library has been updated that the reflectometry profiles stopped unexpectedly moving, up to ten centimeters in extreme cases, and became much more stable, specially during high plasma current ramps. As part of a standard overhaul work to the FLUSH equilibrium access library, a bug that exclusively affected the reflectometry data processing was discovered and fixed. The problem was an unnecessary flux renormalisation step in reading back a Flush-generated file format.

Even after the FLUSH bug-fix and the new LKCO system, the LCFS (Last Closed Flux-Surface) position provided by the equilibrium reconstruction still showed a disagreement to its expected position of

matching the 100 eV from the temperature profile measured with the HRTS (High Resolution Thompson Scattering) diagnostic [6]. The mismatch had been roughly between 2 and 4 centimeters on average and changing for different experimental campaigns. Several enhancements on the equilibrium reconstruction led to a much better agreement, of 1 ± 1 cm, and eliminated the campaign to campaign variation. These enhancements included a probe selection to avoid accounting for faulty probes, the removal of an outdated coil calibration and adding a pressure constraint in the equilibrium reconstruction[7].

All these improvements in the input magnetic field resulted in more stable profile positions and better agreement to other diagnostics, like the interferometry and HRTS. There was still an ≈ 2 cm consistent disagreement to HRTS, which is a diagnostic that is not expected to move radially across different shots or campaigns, but at least this disagreement is consistent, not varying significantly, and expected to be due to the reflectometry reconstruction technique. Given this enhanced position stability, the validation step of reflectometry profiles that adjusted the toroidal magnetic field was discontinued, since they can possibly artificially add unphysical time-dependent effects on the reflectometry profiles.

3 Inner-wall reflection positions

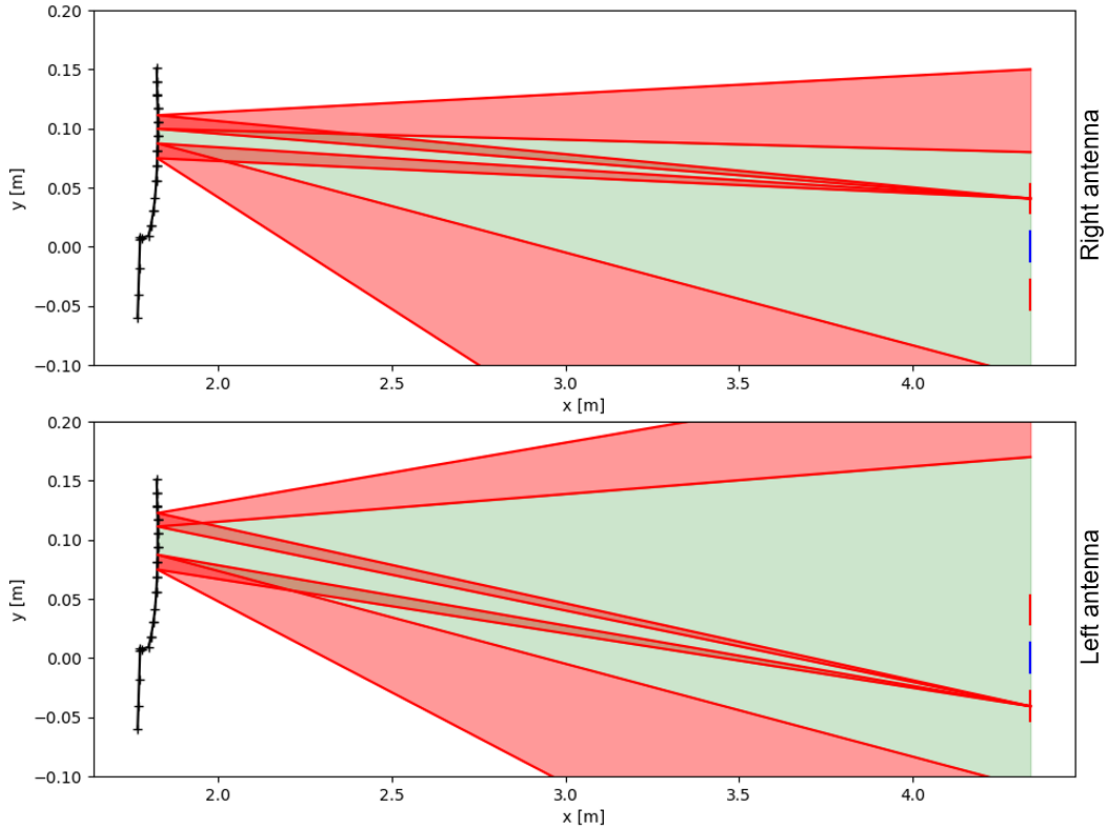

Figure. 1: Ray-tracing of waves injected from left and right open-waveguides. In blue is the center reception waveguide, which only receives waves injected inside the green cone.

The propagation path length during a pre-plasma measurement has been re-assessed due to the complex structure exactly across the reflectometry injection and reception points. The ray-tracing calculations shown in Fig. 1 illustrates how the injected waves are being reflected further out into the limiter instead of just opposite to the injection points. Furthermore, since the probing waves are injected from two open waveguides, each probing band have been assigned a separate path length associated to the waveguide it

goes through. The vertical angle of incident in the wall is also not perfectly 90°, but 88.87°. Nevertheless, the vertical correction is only a decrease of 0.5 mm on the reflection position, which is much smaller than the horizontal correction. The radial inner-wall position changed from the wall guard at 1.78 m to 1.8285 m for the bands going through the left waveguide and 1.833 m for the right waveguide. These are not the exact limiter positions but the numbers that give the equivalent path length considering a straight propagation to simplify the calculation of Eq. 3.

An example of the impact on the reconstructed profiles can be observed in Fig. 2 by comparing the previous case in red to the updated positions in blue. The scrape-off layer profiles don't change significantly, but as the reconstruction goes towards the core, there is an outward shift of $\approx$ 1.5 cm when using the updated inner-wall positions, improving the agreement to the HRTS profile. Furthermore, as can be seen in the pedestal region, around R=3.8 m, there is an oscillation during a band transition, which is eliminated when using the updated band-dependent inner-wall positions.

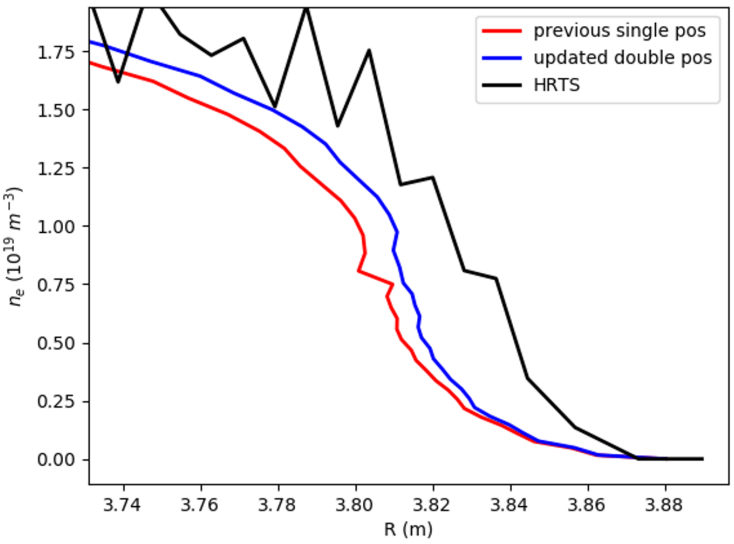

Figure. 2: Example profiles of standard single inner-wall position and updated positions from ray-tracing. Jet pulse 93620, t=52.02s.

4 Ripple effect in the magnetic field profile

As already mentioned in Sec. 1, the reflectometry profiles start very close to the vessel outer-wall, and errors in the input magnetic field profile in the initialization region shift the entire reconstructed profiles. The reflectometry waveguides being located exactly in between two TF (toroidal field) coils, it's expected to experience a lower magnetic field than that extracted from the equilibrium reconstruction. A simple model of each TF coil as a single wire was used to estimate the ripple effect experienced along the reflectometry line-of-sight. For the typical initialization positions between 3.85 and 4 m, the correction on the toroidal field is between 0.15 and 0.4%, respectively.

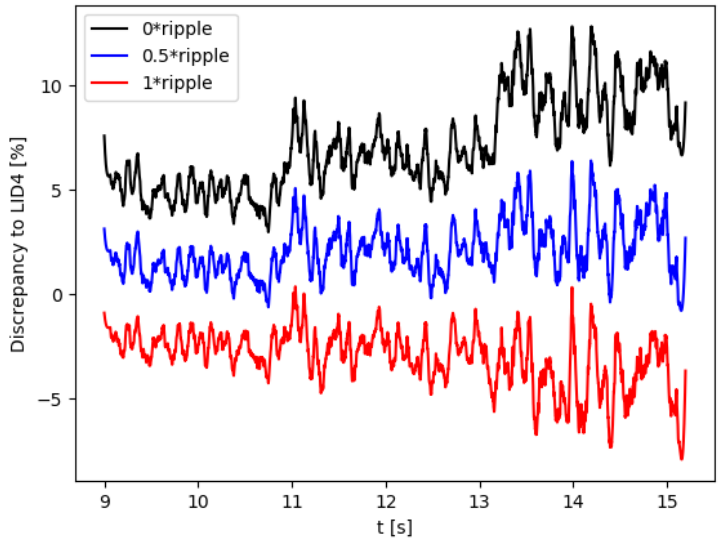

Figure. 3: Comparison of reflectometry agreement to the interferometry LID4 line with varying ripple correction levels, pulse 97297. For clarity, smoothing of 1% of signal length was used.

In order to verify the benefit of including the ripple correction and optimize it's magnitude, Fig. 3

shows the discrepancy between the interferometry LID4 edge line and the reflectometry profiles (integrated along the LID4 line-of-sight), for JET's pulse 97297. This pulse is designed to have three plateaus of the plasma radial outer gap, as can be noticed in the figure. As the ripple correction level is increased from 0%, the reflectometry profiles start agreeing more with the LID4 data, and the agreement becomes more consistent regardless of the plasma position, with the optimal level being just above 50%. This is expected since the single coil assumption is clearly expected to give an overestimation of the ripple correction.

Another test case was performed by changing the initialization position with different levels of ripple correction and observing the changes in profile pedestal position. The results are illustrated in Fig. 4. It's clear that by adding the ripple correction, the pedestal positions move inward, with the effect decreasing as the initialization is done at lower radius. At 3.88 m, the difference between 0% and 100% ripple correction is around 2 mm, whereas at 3.95 m this difference is around 0.6 cm. The fact that the pedestal shows less movement with higher ripple correction level demonstrates that applying the ripple correction is beneficial for the reflectometry profiles. The remaining tendency on the three curves is due to the changing initialization conditions along these positions not related to the f_{ce} profile, like the input phase and amplitude along the initialization probing frequency band and a different n_{e0} along those positions. Lastly, this approach can also be used when investigating a correction curve in n_{e0} to eliminate the remaining tendency, which must be linked to full-wave simulations to understand the amplitude and phase signals or by enforcing any constraint, like agreement to the interferometry edge line. This is possible because, as observed before [8], if the initialization condition is known, even if starting far from the condition $n_{e0} = 0$ (as long as still at the scrape-off layer), the resulting profile error is negligible.

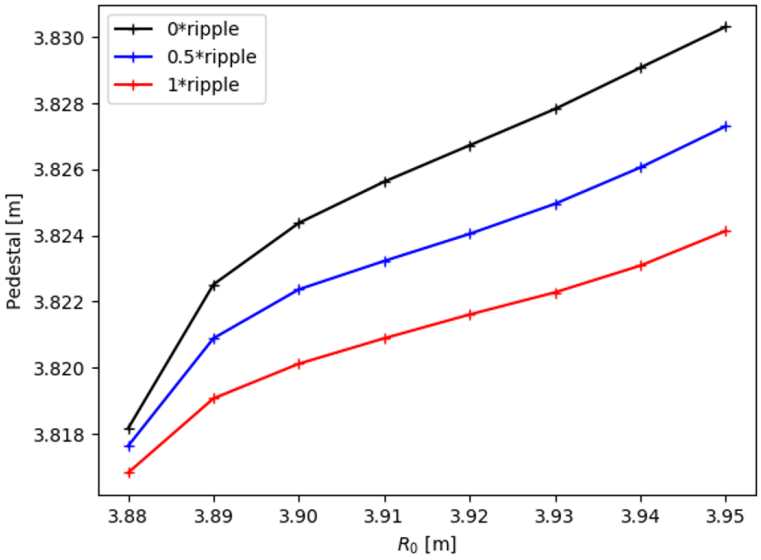

Figure. 4: Reflectometry profile pedestal position with different initialization positions and ripple correction level, at t=12.17s during JET pulse 96098.

5 Optimized sweeping parameters and vacuum fit

Given that reflectometry profiles are more stable given the improvements introduced above, a position benchmark was carried out to observe if any additional trend was still present. No trend was observed for different heating schemes, but the profiles from lower magnetic field discharges showed several additional centimeters of disagreement when compared to the HRTS diagnostic. The problematic field range coincided exactly to the use of the Q-band in the reconstruction algorithm. Upon investigating the sweeping parameters, it was found that the requested sweep-time parameter was being truncated before being passed to the controllers, and the value saved is the requested and not the one set at the controller. This was easily solved by increasing the number of decimal places in the sweep-time parameter. Furthermore, since the

controller interpolates the requests within a database of discreet values, there are small deviations on the requested and the set value depending on the value requested. For example, when requesting a sweep-time of 11 μs, the controller is actually set at 10.97 μs. This mismatch was solved by starting to request values that the controller can set exactly, like the 10.97 μs. The probing band most affected by this issue was the Q-band, as it had by far the highest percentual mismatch in sweeping-time requested, 5.5 μs against the truncated and actually saved 6 μs.

Another optimization implemented was the automatic narrow filtering of the vacuum pre-plasma measurement. This was again specially relevant for the Q-band since it operates at the waveguide lower frequency limit and the signal amplitude compared to the background noise is not as good as for the other bands. Without the filtering, the fit in the vacuum group-delay was easily disturbed by the background noise whenever this band showed any degradation of signal quality.

With both optimizations discussed above implemented, the low field discharges provide density profiles with the same agreement to HRTS as the high field discharges.

6 Burst mode (stacked spectrograms)

For a smooth monotonic density profiles, the reconstruction algorithm can use the instantaneous phase of the reflectometry signal and achieve sub-millimeter accuracy[4]. In practice, due to the high level of turbulence in large-size tokamaks, there's often a high level of spurions reflections. These spurious reflections can cause a significant jitter in the reconstructed profiles. In JET discharges, it's typically in the order of 2 cm for the least affected shots and just over 10 cm for the worst case scenarios, where it also degrades the initialization technique. The burst analysis [5] is the best technique to suppress the spurious events by extracting the phase increment data from the integral of the group delay curve coming from the maximum of stacked spectrograms. After implementing this technique in JET, the profile jitter is strongly suppressed to typically less than a centimeter, specially when stacking at least 4 frequency sweeps. Of course, stacking several frequency sweeps means integrating data over time, so one needs to be bear in mind the averaging effect if the plasma changes within the integration time-frame, which varies for different diagnostic settings.

The use of stacked spectrograms also revealed persistent profile oscillations coming from persistent oscillations in the reflectometry signal. These are likely due to non-linearity of the frequency sweep or influence of secondary side lobes. These oscillations are more evident when probing the plasma sharp pedestal due to the proximity to the waveguides and constant low group delay (in the order of 2 ns). Since these fluctuations are persistent across shots and campaigns, a calibration could be computed (average raw signal over several seconds minus spline fit) for the entire probing

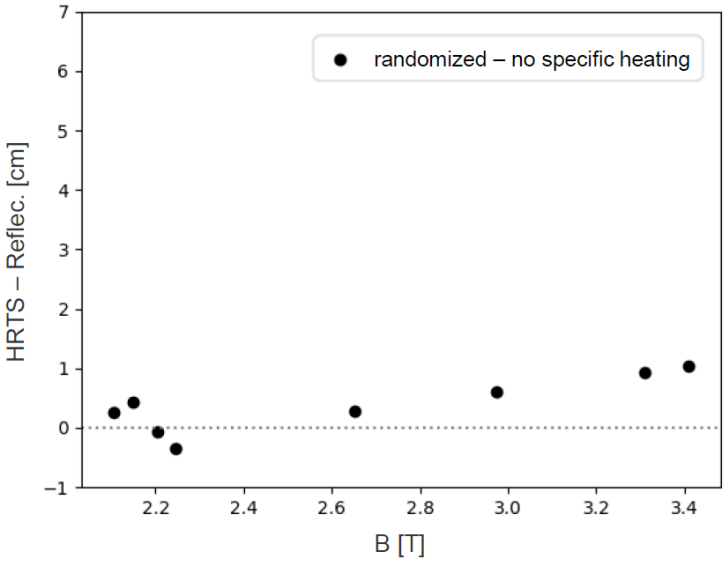

Figure. 5: Benchmark of reflectometry position in comparison to HRTS. The difference is computed at the pedestal center, which is estimated at half of the density at 0.85 normalized radius.

frequency band and they can be subtracted from the main signal. These eliminated strong and unphysical localized profile oscillations.

With all the above improvements in profile reconstruction, another position benchmark was performed. As illustrated in Fig. 5, the reflectometry absolute position is now within ± 1 cm when compared to the HRTS diagnostic, regardless of the heating scheme being used or the background magnetic field. So far, the spectrogram window size isn't yet optimized but roughly adjusted for better agreement to the interferometry LID4. A variable window size spectrogram technique is currently being tested in synthetic data before being implemented to run automatically.

7 Conclusions and prospects

Several aspects of the profile reconstruction technique have been discussed, from the input magnetic field, to updated inner-wall reflection positions, added ripple correction, optimized sweep-time parameter and vacuum fits and implemented the burst mode. All these combined significantly improved the stability and accuracy of the absolute radial position of reconstructed reflectometry density profiles. There are no longer large unexpected profile movements linked to plasma current ramps, strong and persistent oscillations (zig-zags) due to band transition or not, larger discrepancy in low magnetic field and position jitters over several centimeters. They no longer require a correction in the input magnetic field and are now in $\pm$ 1 cm agreement with the HRTS diagnostic. Due to the improved accuracy and robustness, the data has become widely used by the community, specially when a higher temporal resolution is necessary.

Due to the optimization in all these fronts in the reconstruction data analysis and minimization of their error contributions, it's now possible to experimentally investigate improvements in the initialization technique, be it with techniques based on synthetically analysed signals, or by improving agreement to other diagnostics.

References

[1] A. Sirinelli *et al.*, Rev. Sci. Instrum. **81**, 10D939 (2010).

[2] Bottollier-Curtet, PhD thesis, Université de Paris (1986).

[3] D. A. Shelukhin *et al.*, IRW11 (2011).

[4] R. B. Morales *et al.*, Rev. Sci. Instrum. **88**, 043503 (2017).

[5] P. Varela *et al.*, Rev. Sci. Instrum. **46**, S693 (2006).

[6] Simpson *et al.*, Nucl. Mater. Energy **20** 100599 (2019).

[7] G. Szepesi *et al.*, 47th EPS Conference on Plasma Physics (2021).

[8] R. B. Morales, PhD thesis, Universite de Lorraine (2018).

Acknowledgments

This work has been carried out within the framework of the Contract for the Operation of the JET Facilities and has received funding from the European Union's Horizon 2020 research and innovation programme. It's also been partly carried out within the framework of the EUROfusion Consortium, funded by the European Union via the Euratom Research and Training Programme (Grant Agreement No 101052200 — EUROfusion) and from the EPSRC [grant number EP/W006839/1]. Views and opinions expressed are however those of the author(s) only and do not necessarily reflect those of the European Union or the European Commission. Neither the European Union nor the European Commission can be held responsible for them.